INTERNATIONAL SOCIETY FOR
SOIL MECHANICS AND
GEOTECHNICAL ENGINEERING

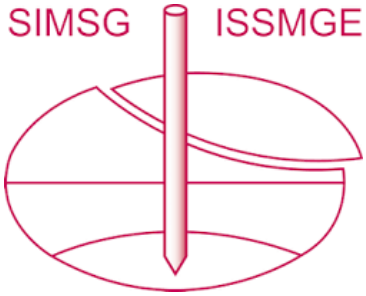

This paper was downloaded from the Online Library of the International Society for Soil Mechanics and Geotechnical Engineering (ISSMGE). The library is available here:

https://www.issmge.org/publications/online-library

This is an open-access database that archives thousands of papers published under the Auspices of the ISSMGE and maintained by the Innovation and Development Committee of ISSMGE.

Evaluation of in-situ saturation condition for an unsaturation method for liquefaction countermeasures

H. Nakazawa
Earthquake Disaster Mitigation Research Division, National Research Institute for Earth Science and Disaster Resilience, Japan

T. Takagi
Fukken Co., Ltd., Japan

H. Hayashi
Geo-X Consultants Co., Ltd., Japan

K. Tabata
National Research Institute for Earth Science and Disaster Resilience, Japan

K. Nagao
Sato Kogyo Co., Ltd., Japan

ABSTRACT: The Tohoku Earthquake caused significant damage in residential areas due to liquefaction. After the earthquake, several liquefaction countermeasures were developed and one of these countermeasures is an unsaturation method. But there are few techniques for quantitatively estimating the in-situ effectiveness of this technique. In this study, a series of tests were performed on unsaturated models to develop estimation procedures for in-situ conditions. We used travel time tomography to obtain P-wave velocity distributions by utilizing data from dynamic cone penetration tests, and the cone was used as a vibration source. Travel time tomography was then performed using mini-ram sounding to obtain P- and S-wave velocity distributions after in-situ standard penetration and PS-logging tests. Finally, the P- and S-wave velocity distributions were converted into *B*-value distributions estimated from Biot's porous elasticity theory. The results show that the proposed method is effective for evaluating in-situ saturation conditions.

1 INTRODUCTION

The 2011 Tohoku Earthquake caused major destruction along the Pacific coast of Japan, and a large amount of damage due to liquefaction was reported in residential areas in the Kanto Plane region. As a result, various countermeasures against liquefaction including the unsaturation method have been developed (Urayasu city, 2012). This involves directly injecting air into the liquefiable soil layer or replacing ground water with micro bubble water (MB-water), as shown in Figure 1 to increase the liquefaction resistance (Nagao et al. 2015). The MB-water contains air bubbles with diameters ranging from 10 to 100 μm. The use of this method reduces construction costs and space, and is more environmentally friendly than other techniques, but requires in-situ monitoring of saturation conditions such as the degree of saturation (S_r) and the pore water parameter (B-value) of the countermeasure layers to determine the effectiveness of the procedure.

It is widely known that the liquefaction resistance (R_l) increases as S_r decreases (Yoshimi et al. 1989). Figure 2 shows that the liquefaction resistance (R_u/R_s) of unsaturated soils increases with decreasing P-wave velocity (V_p) and B-value. As shown in Figure 2(a), R_u/R_s of fully saturated soils increases by a factor of 2 at V_p = 450 m/s, as measured using a triaxial test apparatus equipped with bender elements (BE) for elastic wave velocity measurement (Nakazawa et al. 2004). Ground investigations such as the standard penetration test (SPT) and the dynamic cone penetration test (DCPT) can also be used for the design of liquefaction countermeasures.

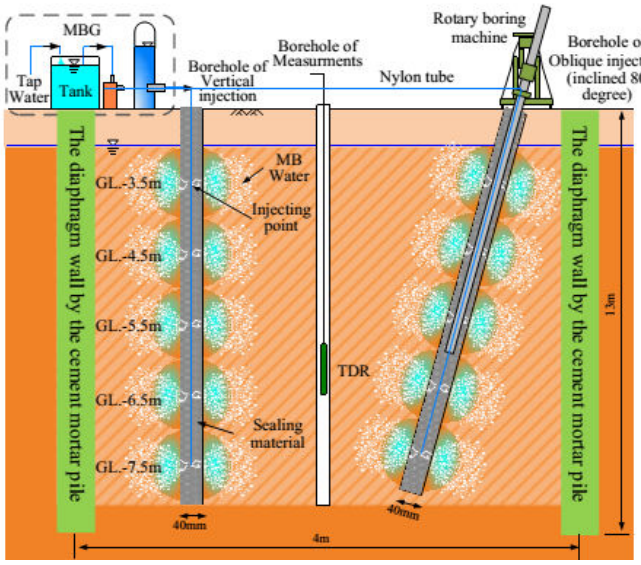

Figure 1. MB water injection.

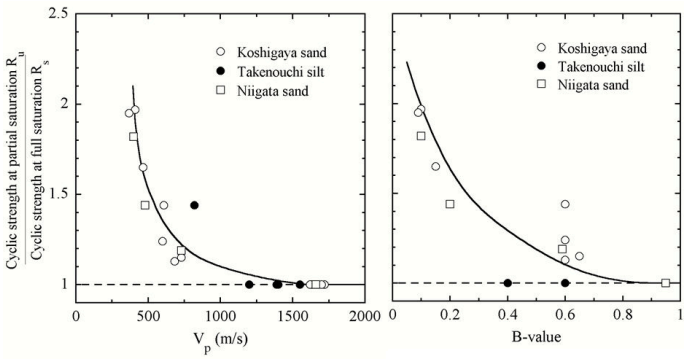

(a) R_u/R_s versus V_p (b) R_u/R_s versus V_s

Figure 2. Liquefaction resistance of unsaturated sandy soil.

We aim to develop techniques for the estimation of in-situ saturation conditions using a combination of ground investigations and physical exploration. In this study, we investigate the use of travel time tomography to obtain P- and S- wave velocity distributions from cone penetration tests.

2 EVALUATION OF UNSATURATED GROUND IN TEST MODEL

2.1 *Outline of laboratory model tests*

Laboratory tests were performed using cone penetrometer equipment and in-situ saturation conditions monitored by installing an observation borehole at the MB-water improvement site to enable for periodic observations. However, it is difficult to evaluate the saturation conditions around the observation borehole and maintain its function. The distribution of elastic waves that occurs due to cone penetration in the model ground was measured to obtain the two-dimensional saturation conditions.

2.1.1 *Soil properties and model ground*

Figure 3 shows a schematic diagram of the test model. The model ground was prepared in a steel container measuring 3 m long, 0.6 m wide and 1.0 m deep. Iide silica sand was used as the model ground. Table 1 shows the physical properties of Iide silica sand. The density of the soil particles (G_s) was 2.621 g/cm^3, the maximum and minimum void ratios (e_{max} and e_{min}) were 0.858 and 0.543 respectively, the mean particle size (D_{50}) was 0.299 mm, and the uniform coefficient (U_c) was 2.2.

At first, model ground with of relative density (D_r) of 60% was made using the air pluviation method to uniformly distribute the dry sand in the container. The model ground was then gradually saturated using de-aired water permeation from the bottom of the container toward the surface. Finally, the pore water was replaced by MB-water using the same technique.

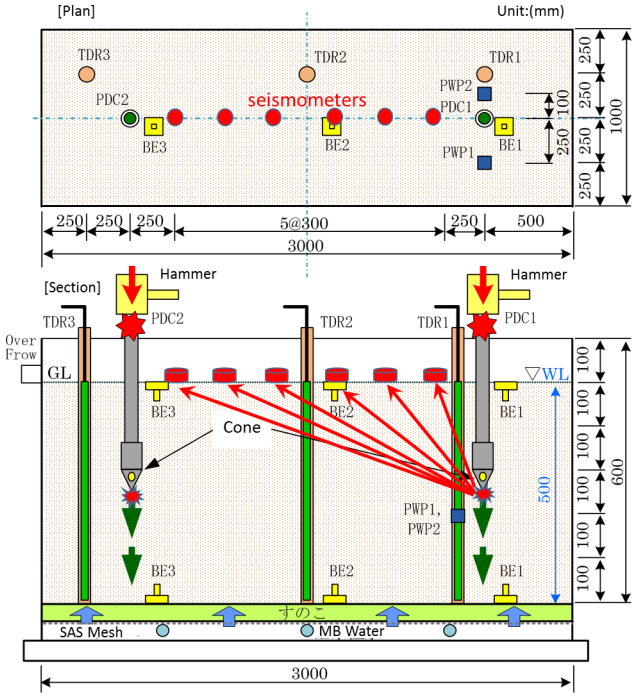

Figure 3. Schematic diagram of the test model.

Table 1. Properties of Iide silica sand.

Density of soil particles	ρ_s	(g/cm^3)	2.651
Maximum grain size	D_{max}	(mm)	0.850
Fine content (<0.075 mm)	F_c	(%)	0.7
Mean particle size	D_{50}	(mm)	0.299
Uniform coefficient	U_c		1.778
Minimum density	ρ_{dmin}	(g/cm^3)	1.413
Maximum density	ρ_{dmax}	(g/cm^3)	1.744
Maximum void ratio	e_{max}		0.876
Minimum void ratio	e_{min}		0.520

2.1.2 *Test apparatus*

The piezo drive cone (PDC) test was used because it acquires data related to the pore water pressure, *N*-value, groundwater level, fine content, etc. As shown in Photograph 1, the cone top angle was 60º and the diameter 36.6 mm. It was equipped with a pore water pressure sensor and a rod 28 mm in diameter (Sawada, 2004). In this study, a simplified PDC test was performed by driving the rod with a 2.5 kg hammer.

The vibration travel time was calculated using six seismometers installed at 30 cm intervals on the ground surface. Using this information, two-dimensional P-wave velocity distributions were obtained for dry, saturated and unsaturated conditions. A geophone with a natural frequency of 4.5 Hz was used to record the vibrations.

Photograph 2 shows the test model and the simplified PDC penetration apparatus. Both time-domain-reflectometry soil-moisture meter (TDR) and variable energy dynamic cone penetrometer (VEDCP) tests were performed using the simplified PDC apparatus. The TDR tests were conducted to obtain the average value of S_r because the length of the probe was 30 cm, which approximates the ground thickness. A VEDCP is a portable cone

penetrometer used for evaluating soil strength and every penetration is usually 1 to 2 cm. (Langton, 1999).

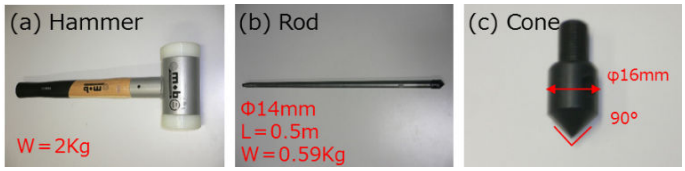

(a) hammer (b) extension rod (c) cone
Photograph 1 VEDCP apparatus

(a) Seismometers (b) simplified PDC
Photograph 2. Test model

2.2 *P-wave velocity distribution in dynamic cone penetration*

2.2.1 *Testing program and model ground*

After air pluviation, the 500 mm model ground was gradually saturated with de-aired water permeation from the bottom of the container up before the pore water was replaced with MB-water using the same methodology. It was confirmed that S_r reached approximately 90% by TDR. The distribution of cone penetration resistance (q_d) by VEDCP shown in Figure 4 indicates similar tendencies under saturated and unsaturated conditions around PDC1 and PDC2, as shown in Figure 3. From the results of the BE measurements, the average V_p is 180 to 190 m/s in dry sand, 900 to 1000 m/s in saturated sand and 200 to 220 m/s in unsaturated sand.

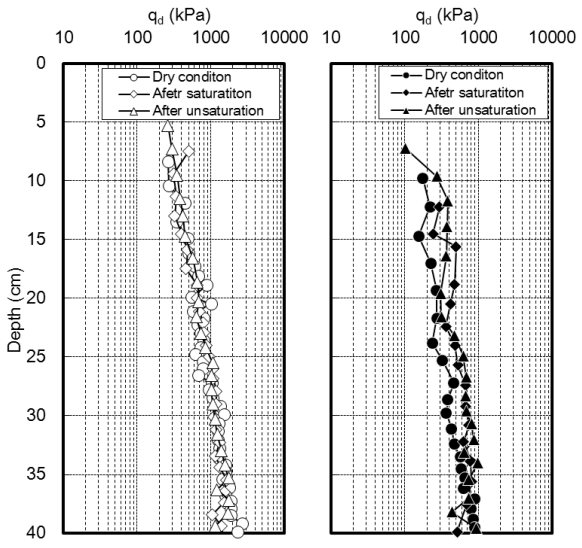

(a) Around PDC1 (b) Around PDC2
Figure 4. Results of VEDCP tests

2.2.2 *Travel time tomography for P-wave velocity distribution*

The simplified PDC test was performed from the ground level to the bottom and elastic waves measured at 5 cm intervals. Figure 5 illustrates sections of 2-D P-wave velocity distributions based on travel time. The value of V_p is less than 160 m/s in shallower layer than GL.-0.25m in dry sand. In addition, V_p below the ground surface in saturated sand increases to more than 200 m/s. After the introduction of the MB-water, local increases and decreases of V_p were observed. In particular, it was observed that V_p decreases at depths of GL.-35cm and GL.-15cm. It is suggested that non-uniformity of MB-water permeation and the influence of density changes cause these variations. However, it can be seen that these results were almost harmonized with the average V_p measured by BE.

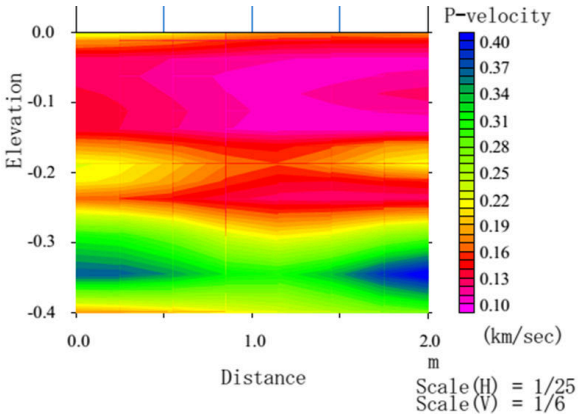

(a) Dry sand

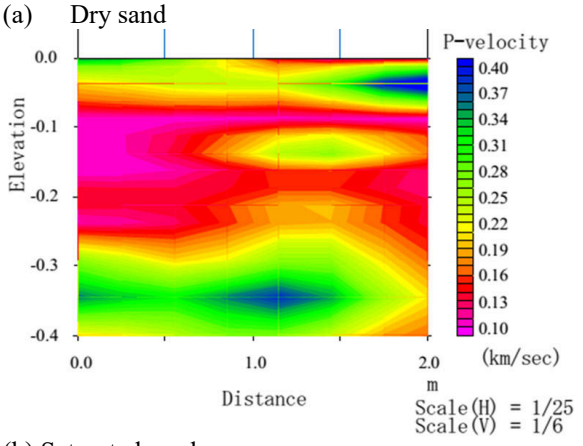

(b) Saturated sand

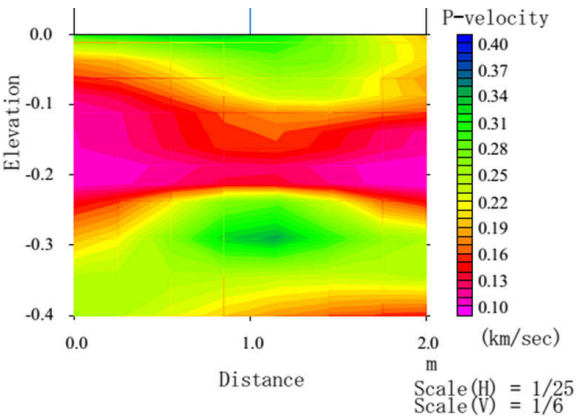

(c) After injection of MB-water (S_r=90%)
Figure 5. V_p distributions.

3 CASE STUDY - TOMOGRAFY ANALYSIS USING DYNAMIC PENETRATION TEST

The results show that P-wave tomography is possible using a cone and hammer as the vibration source. In order to develop this technique for in-situ investigations, mini-ram sounding (MRS) tests were conducted. The MRS specification is shown in Table 2.

Table 2. Main specification of MRS.

Hammer	Mass, m(kg)	30
	Falling hight, H (mm)	350
Cone	Diameter, D_c (mm)	36.6
	Top angle (°)	90
Rod	Diameter, D_r (mm)	28
Energy per unit area	E_n=mgH/A (kJ/m^2)	98
Operation	-	Automaticallydropping a hammer
Penetration resistance	-	Blow counts at every 20cm
Skin friction	Torque, M_v (Nm)	Rotetion of rod at every 100cm

3.1 *Outline and procedure of field investigation*

The test field (see Figure 6) for the in-situ investigations was located at the National Research Institute for Earth Science and Disaster resilience (NIED) in Japan. After SPT and PS-logging, 6 seismometers were installed at intervals of 1.5 m on the ground surface, as shown in Figure 7, and MRS tests were performed to record the travel time of vibrations generated by the cone. MRS tests were performed at 2 points on the seismometer measurement line.

Figure 6. Investigation site at NIED

3.2 *Measurement method*

Any analysis of travel time tomography requires for precise data. Therefore, 1 m reinforcing rods were inserted at every observation point to amplify the sensitivity of the seismometers. The installation of a seismometer is shown in Figure 7. A seismometer was used as a trigger every 50 cm between GL.-4 m and GL.-8 m below the ground water and vibrations generated by MRS blows.

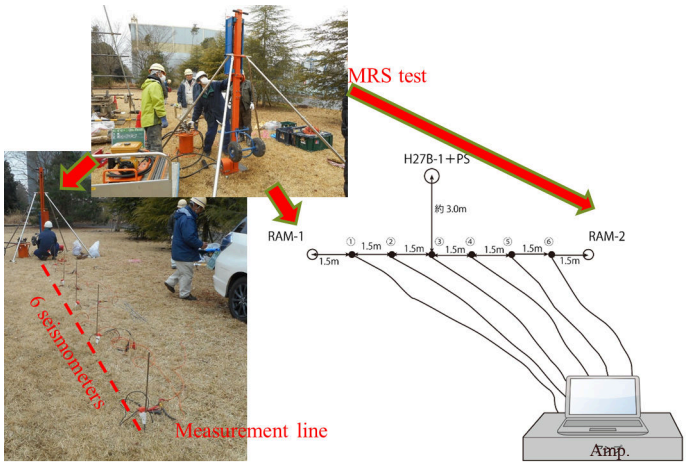

Figure 7. Travel time tomography using MRS test.

3.3 *Results of investigations*

The investigation site was located at the boundary between a hill and lowland area and consisted of a loam layer and alternating strata of sandy soil and clay. The sandy soil layer was a deposit of old river course and the clay stratum equivalent to a mud layer of backswamp. Ground water was confirmed around GL.-3 m.

Figure 8 and Table 3 show the results of the ground investigation and the physical properties of the sandy soil layer, respectively. The depth of the sandy soil layer, which was assumed to be the liquefiable layer, was GL.-4.0 to GL.-5.35 m. The distribution of N-values in this layer is 2 to 4 and V_p and V_s 970 m/s and 200 m/s respectively. Blow counts (N_m) were measured every 20 cm. The torque (M_v) was measured every 100 cm so that skin friction could be accounted for. The N-value (N_d) was calculated using the following equations.

$$N_d = 0.5N_m \quad \text{for sandy soil} \tag{1a}$$

$$N_d = 0.5N_m - 0.016M_v \quad \text{for cohesive soil} \tag{1b}$$

It was assumed that the results correspond to a change in the stratum continuity according to the comparison shown in Figure 8.

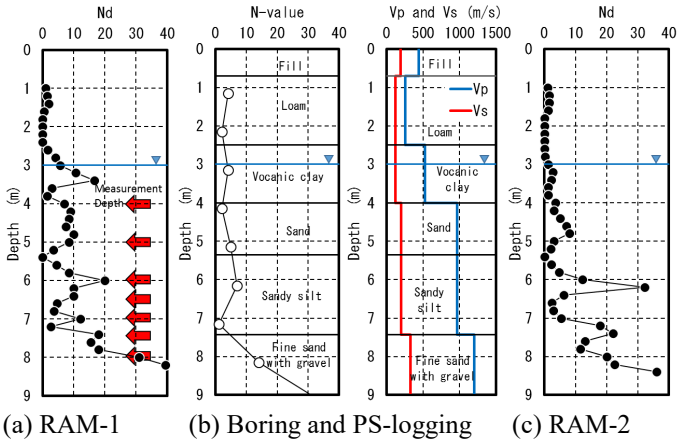

(a) RAM-1 (b) Boring and PS-logging (c) RAM-2

Figure 8. Results of SPT, PS-logging and MRS tests.

Table 3. Properties and indices of sand layer at GL.-5.3m

Density of soil particles	ρ_s	(g/cm^3)	2.680
Grain size distribution			
Gravel content (> 2 mm)		(%)	0.0
Sand content (≤ 2 mm)		(%)	92.3
Silt content (≤ 75 μm)		(%)	1.9
Clay content (≤ 2 μm)		(%)	5.8
Mean particle size	D_{50}	(mm)	0.240
20% particle size	D_{20}	(mm)	0.140
10% particle size	D_{10}	(mm)	0.120
Water content (%)	w_n	(%)	31.0
Plasticity index (%)	*Ip*		NP

3.4 *Distribution of elastic wave velocity*

Vibrations were measured during the MRS tests every 50 cm or 100 cm below GL.-4.0 m to identify both P- and S-waves as shown in Figure 9.

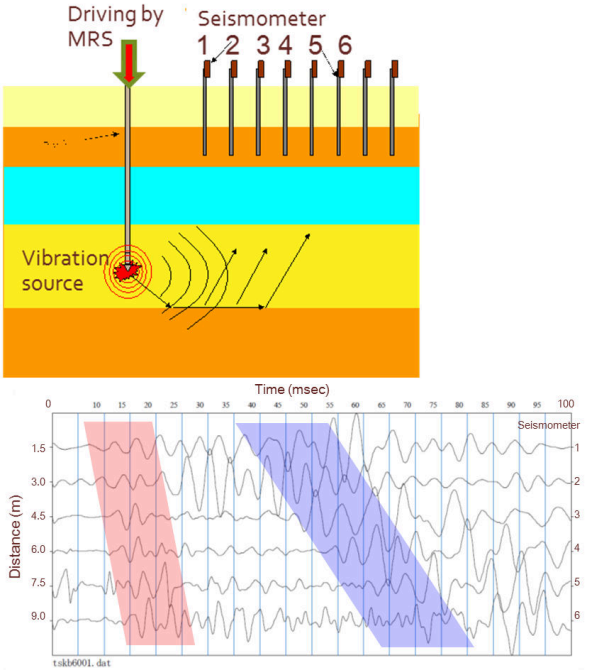

Figure 9. An example of elastic waves generated at the depth of GL.-4m by MRS test.

The travel time based on the initial P-wave forms was determined from this figure before the 2-D P-wave distribution was obtained from the P-wave tomography analysis shown in Figure 10, which shows the stratum aspect with the results of other investigations. It can be seen that a 2-D P-wave distribution evaluated by tomography analysis does not correspond with the MRS tests results at the start and end points (RAM-1 and RAM-2) on the measurement line.

The identification of P-waves from measured wave forms is a common task, but the identification of S-waves is often ignored. We recorded the initial S-wave motions using the wave forms measured for the P-wave tomography and S-wave tomography analysis was performed. The 2-D S-wave distribution from the S-wave tomography is indicated in Figure 11. Generally, it is well known that S-wave velocity correlates with shear modulus. Therefore, V_s tends to express the actual soil layer distribution. It is suggested that the 2-D S-wave velocity distribution is harmonized with a soil layer at the boring investigation point during SPT and PS-logging.

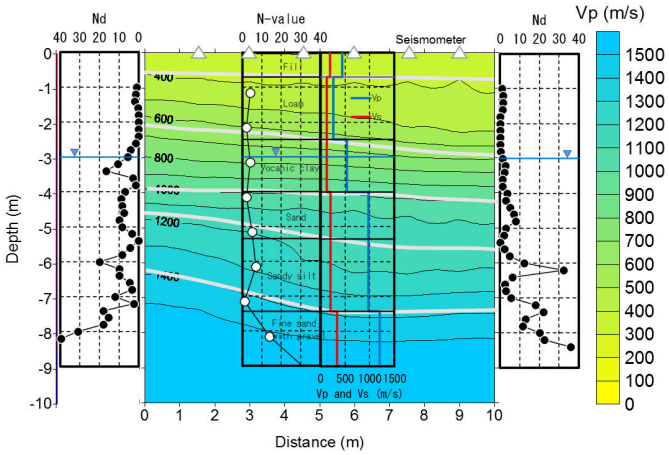

Figure 10. 2-D P-wave distribution.

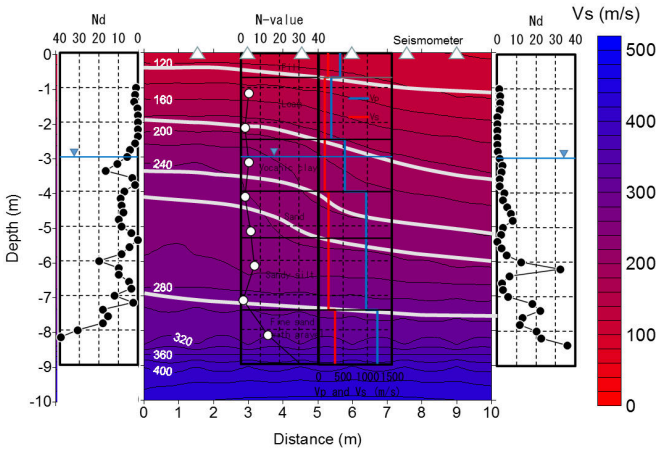

Figure 11. 2-D S-wave distribution.

4 EVALUATION OF IN-SITU SATURATION CONDITIONS

Finally, the 2-D elastic wave (P- and S-wave) velocity distributions could be obtained from the tomography analysis. In order to interpret the in-situ saturation conditions, the P- and S-wave distributions were converted into a *B*-value distribution, based on Biot's porous elasticity theory. The *B*-value was adopted as an in-situ estimation index because the liquefaction strength of unsaturated soil can be expressed as a function of *B*-value as shown in Figure 2(b) and subtler changes in saturation conditions can be more easily identified (Nakazawa et al. 2004).

4.1 *The poro-elastic theory*

It is proposed that the relation between *B*-value and V_p under unsaturated conditions can be clarified using the bulk modulus of water, soil particles and the soil skeleton. Based on Biot's theory on water-filled porous elastic materials and the poro-elastic theory developed by Ishihara (Biot, 1956; Ishihara 1968), the structure of the sand deposit is equivalent to a poro-elastic body saturated with water and can be

represented as a function of V_p/V_s, ν_b and B-value according to the following equation:

$$\left(V_p/V_s\right)^2 = \frac{4}{3} + \frac{2(1+\nu_b)}{3(1-2\nu_b)(1-B)} \quad (2)$$

where ν_b is the Poisson's ratio of the soil skeleton. Tsukamoto et al. (2002) reported that it is appropriate to assume the value of ν_b = 0.35 for general sands.

It therefore becomes possible to estimate in-situ B-value by substituting the elastic wave velocities obtained from ground investigation such as PS-logging into equation 2.

4.2 *B-value distribution*

Figure 12 indicates the 2-D B-value distribution estimated using Equation 2 based on Figures 10 and 11. The B-value distribution area is shown below GL.-3 m.

It can be seen that B-values are comparatively high at the investigation site. However, considering the sandy soil layer, it cannot be confirmed that the B-value increases, but variation can be observed. Specifically, the B-value is between 0.80 and 0.85 and slightly lower near the MRS1 side. Conversely, it is greater than 0.9 in saturated conditions and approaches saturated conditions near the MRS2 side.

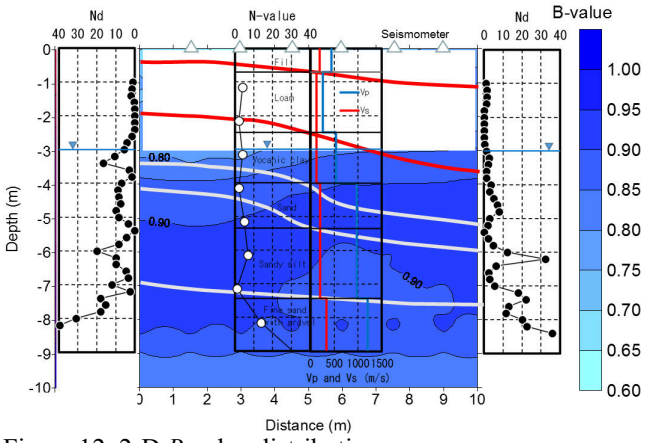

Figure 12. 2-D B-value distribution.

Though the results shown in Figure 12, which is B-value is smaller than 1.0 even below the groundwater table of GL.-3m, were obtained from the in-situ investigation, liquefaction resistance has been usually evaluated in sandy soils or liquefiable layers with B-value of more than 0.95. The distribution of the predicted B-value in sandy soil layer in the investigated site were almost between 0.8 and 0.9. Based on Figure 2(b), there is almost indicated no increase in liquefaction resistance. It is considered that it is a reasonable result that the liquefaction resistance hardly increases because the investigated site was not improved but natural ground. At least an increase in liquefaction resistance is significant in B-value range less than 0.6, and V_p at B-value of 0.6 is equivalent to about 1000 m/s as shown in Figure 2(a). On the other hand, S_r showed 90% in the MB-improved ground in Figure 5(c) and Urayasu site reported by Nagao was the same. In this case, liquefaction resistance will be about twice compared to saturated state because it is assumed that the B-value becomes close to 0.0. Therefore, it is thought that it is better to verify this technique in MB-improved site.

5 SUMMARY

In this study, we tried to develop an estimation procedure for in-situ saturation conditions based on laboratory tests on unsaturated soils and travel time tomography utilizing dynamic cone penetration tests for quantitatively estimating the in-situ effectiveness of unsaturation method for liquefaction countermeasure. The results of the model tests and in-situ tomography show that the application of physical exploration for elastic wave velocity by MRS tests can be effective for analyzing in-situ saturation conditions. However, it is necessary to assess the accuracy of the technique using in-situ investigations in unsaturated ground including MB-improvement.

6 REFERENCES

Biot, M.A. 1956. Theory of propagation elastic waves in a fluid-saturated porous solid, *Journal of Acoustical Society of America*, 28(2): 168-191.

Ishihara, K. 1968. Propagation of Compressional Waves in a saturated soil, *Proceeding of the International Symposium of Wave Propagation and dynamic Properties of Earth Material*: 195-206.

Langton, D.D. 1999. The Panda lightweight penetrometer for soil investigation and monitoring material compaction. *Ground Engineering, September*: 33-37.

Nagao, K., Suemasa, N., Jinguji, M. & Nakazawa, H. 2015. In-situ applicability test of soil improvement for housing sites using Micro-Bubbles against soil liquefaction in Urayasu, Japan. *Proceedings of 25th International Ocean and Polar Engineering Conference*: 845-852.

Nakazawa, H., Ishihara, K., Tsukamoto, Y. & Kamata, T. 2004. Case studies on evaluation of liquefaction resistance of imperfectly saturated soil deposits. *Proceedings of Cyclic Behaviour of Soils and Liquefaction Phenomena*: 295-304.

Sawada, S. 2004. Estimation of liquefaction potential using dynamic penetration with pore pressure transducer, *Proceedings of Cyclic Behaviour of Soils and Liquefaction Phenomena*: 305-312.

Tsukamoto, Y., Ishihara, K., Nakazawa, H., Kamada, K. & Huang, Y. 2002. Resistance of Partly Saturated Sand to Liquefaction with Reference to Longitudinal and Shear Wave Velocities, *Soils and Foundations* 42(6): 93-104.

Urayasu city. 2012. Liquefaction of measures realization possibilities Technology Committee. http://www.city.urayasu.lg.jp/shisei/johokoukai/shingikai/toshiseibi/1002853/index.html. (Viewed at 2017.9.26)

Yoshimi, Y., Tanaka, K. & Tokimatsu, K. 1989. Liquefaction resistance of a partially saturated sand. *Soils and Foundations* 29(3): 157-162.